Soft Matter

Influence of Aerogel Mechanical Properties on Collagen Micromorphology and its Architecture

Journal:	*Soft Matter*
Manuscript ID	SM-ART-10-2024-001158.R1
Article Type:	Paper
Date Submitted by the Author:	21-Dec-2024
Complete List of Authors:	Rodriguez Sala, Martina; The University of Memphis, Physics and Materials Science Skalli, Omar; The U of Memphis, Biological Sciences Chandrasekaran, Swetha; Lawrence Livermore National Security LLC, Worsley, Marcus; Lawrence Livermore National Laboratory, Physical and Life Sciences Directorate Leventis, Nicholas; Aspen Aerogel Sabri, Firouzeh; University of Memphis, Physics; UofM, physics and Materials Science

SCHOLARONE™
Manuscripts

Please do not adjust margins

ARTICLE

Influence of Aerogel Mechanical Properties on Collagen Micromorphology and its Architecture

Received 00th January 20xx,
Accepted 00th January 20xx

DOI: 10.1039/x0xx00000x

Martina Rodriguez Sala[a], Omar Skalli[b] Swetha Chandrasekaran[c], Marcus Worsley[d], Nicholas Leventis[e] and and Firouzeh Sabri[f]

Previously, we demonstrated the promise of aerogels for the repair of nerve injuries as neural cells extend longer processes (neurites) when grown on aerogels compared to control surface. We also reported that the aerogel surface topography influenced neurite length. Neurite extension may be boosted by depositing collagen on the aerogel prior to plating the cells. Indeed, collagen has many applications in biomaterials for nerve repair because it profoundly influences cellular properties such as shape and motility. Using collagen to enhance neurite extension requires knowing the effect of collagen deposition on the aerogel surface profile as well as how the aerogels surface topography influences collagen organization into fibers or films. Herein, we have examined by SEM and profilometry the reciprocal relationship between collagen micromorphology and aerogel surface features including pore diameters, surface roughness and Young's modulus (Y). Using 5 types of aerogels differing from each other by these parameters, we show that increasing the collagen surface concentration from 4 to 20 µg/cm2 leads to a gradual transition in collagen architecture from discrete fibers to films where individual fibers were not discernible. The collagen surface concentration at which deposited collagen changes from filaments to films (Transition Point, T.P.) was strongly dependent on aerogel physical properties as it increased with increasing pore diameter and surface roughness, while Y had little effect. These results provide a practical framework to customize the organization of collagen fibers on scaffolds for biomedical applications.

1. Introduction

Collagen, the most abundant protein in vertebrates, accounts for about a third of the mass of human proteins [1]. It is also the most prevalent component of the extracellular matrix (ECM) and plays a key role in cell-ECM interactions and in determining the mechanical properties of tissues and organs [2-4]. Of the 20 distinct types of collagens identified to date, collagen type I is the most widespread and its biochemistry, structure and assembly have been extensively investigated [1], [5]. Collagen binds to transmembrane receptors such as integrins and discoidin domain receptors [6]. These receptors are connected to the cytoskeleton on their cytoplasmic side [7] and their binding to collagen influences cytoskeletal organization and dynamics as well as signal transduction pathways are essential for cell adhesion, cell shape, motility proliferation [8-15] and response to growth factors [16].

Because of collagen's profound influence on cells and tissue organization, and the ease of extracting collagen in large quantities from tissues [1], [5], it has been used abundantly in biomaterials. Given that biomaterials in general lack the cues from the ECM, specifically those providing much-needed adhesion to the substrate and activation of signalling pathways for cell survival and differentiation [17], the collagen layer becomes an integral part of the assembly. Collagen's broad biomedical applications range from drug delivery to tissue engineering and scaffolding design for 3D cell culture systems [14], [18-20]. Collagen has also been combined with electrospinning techniques involving nanofibers for cartilage and bone regeneration applications [21].

Our group has previously shown that the extension of neurites by neuronal cells grown on aerogels depends on the roughness of the aerogel surface and on its Young's modulus [11]. More generally, it is well-established that cells respond to substrate topography, roughness, and rigidity by showing distinctly different behaviors on filamentous surfaces compared to continuous, film-like surface [22,23]. These differences affect cell spreading, alignment, migration, and contact guidance, which are behaviors important to consider when designing materials for tissue engineering therapeutic applications [24-26].

The promise of aerogels as a biomaterial for nerve repair and regeneration has been previously reported by our group [24],

[a,a] mrdrgzsl@memphis.edu, Department of Physics and Material Science, The University of Memphis, Memphis, Tennessee, 38152.
[b,b] oskalli@memphis.edu Department of Biological Sciences, The University of Memphis, Memphis, Tennessee, 38152.
[c,c] chandrasekar2@llnl.gov Lawrence Livermore National Laboratory, Livermore, CA 94550, USA.
[d,d] worsley1@llnl.gov Lawrence Livermore National Laboratory, Livermore, CA 94550, USA.
[e,e] nleventis@aerogel.com Research and Development, Aspen Aerogels Inc., Northborough, MA, USA
[f,f†] fsabri@memphis.edu, Department of Physics and Material Science, The University of Memphis, Memphis, Tennessee, 38152.
† Corresponding Author

Please do not adjust margins

[27-32]. Both biostable and biodegradable aerogels have consistently outperformed other types of biomaterials for smart and passive neural implants [9-12], [24], [28], [33-37]. Furthermore, aerogels have the added advantage that they can be non-invasively tracked in the body making these materials more attractive than other materials for future biomedical applications [38], [39]. Recent developments in the fabrication of biodegradable aerogels have further cemented the notion that aerogels are a suitable material for several biomedical applications [24], [36], [40], [41].

A key step in the preparation of aerogels for seeding with cells is the prior deposition of a collagen layer [9-12], [33-35]. We have previously shown that the deposition of this collagen layer is affected by the aerogel surface features and that this in turn affects cell behavior [10], [33]. Given that aerogels vary in stiffness, surface roughness, pore size, and tortuosity, it is necessary to fully characterize the collagen-aerogel interface and its surface profile. While the effect of temperature on collagen deposition has been reported [42], the effect of the aerogel surface architecture and physical properties on the structure of the deposited collagen layer is lacking.

In this work, we have used different types of aerogels (PCSA, BRF-CA, SSMPA Mix14, SSMPA Mix18, and ARF-CA) to investigate the effect of their surface characteristics on the micromorphology of deposited collagen layers. The various aerogels differed in pore diameter (0.5 to 15 µm), surface roughness (0 to 2 µm) and Young's modulus (0 to 1.5 MPa). Collagen type I of increasing concentration was deposited on these aerogels and two distinct outcomes were observed, namely the deposited collagen layer appeared as discrete fibers or as a continuous film. This study systematically explores the relationship between the structure of collagen deposits and the characteristics of the aerogel surface and defines a parameter, the turning point (T.P.) characterizing the transition from a filamentous to a sheet morphology.

2. Materials and Methods

2.1 Aerogel Synthesis and Preparation

For this study, five different types of aerogels were chosen to cover the full spectrum of pore size, roughness, and stiffness. The types of aerogels included acid-catalysed resorcinol formaldehyde carbon aerogel (ARF-CA), base-catalysed resorcinol formaldehyde carbon aerogel (BRF-CA) [43-45], polyurea crosslinked silica aerogel (PCSA) [11], [24], [33], and superelastic shape memory polyurethane aerogels (SSMPA) Mix14 and Mix18 [46], [47]. For these aerogels, pore diameter (p) varied from 0 to 15 µm, surface roughness (Sa) covered the range of 0.5-2 µm, and Young's modulus (Y) covered the 0-1.5 MPa range. Table 1 summarizes the main properties of the aerogels used in this study.

Polyurea crosslinked silica aerogels (PCSA) were prepared as described previously [11], [24], [33]. Briefly, methanol, deionized water, tetramethyl orthosilicate **(**Sigma-Aldrich, St. Louis, MO) and (3-aminopropyl) triethoxysilane (Sigma-Aldrich) were mixed to form a colloidal suspension. This suspension was washed and cross-linked for 24 hrs with Desmodur N3200 (Bayer Material Science, Leverkusen, Germany) and acetonitrile (Sigma Aldrich). The gels were then placed in multiple baths of acetonitrile and critically point dried (CPD).

Carbon aerogel coupons were synthesized from resorcinol and formaldehyde with water and either acetic acid or sodium carbonate to form gels that were cured, soaked in acetone, and critically point dried [43, 44]. The aerogels were then heated under nitrogen atmosphere with a slow heating and cooling rate [45].

Table 1. Properties of aerogel types used in this study.

	Chemical Components (mol/mol)	Bulk density ρ (g/cm³)	Porosity (% void)	Pore diameter d (mm)	Elastic Modulus Y (MPa)
PCSA	Tetramethyl orthosilicate, 3-aminoprophyl triethoxysilane, Desmodur N3200 [10]	0.7 [10]	70 [10]	0.5 [10]	3MPa [10]
BRF-CA	0.0056 mol resorcinol, 0.011 mol of 37% formaldehyde solution, 3mg of sodium carbonate. [9]	0.153 +/-0.002 [10], [43-45]	93	0.5 [10]	1000 [43], [44], [45]
SSMPA Mix-14	1 triethylene glycol[46], [47]	0.63 [46], [47]	56.1 [46], [47]	2.05 [46], [47]	0.79 [46], [47]
SSMPA Mix-18	0.25 diethylene glycol, 0.5 triethylene glycol, 0.25 tetraethylene glycol [46], [47]	0.61 [46], [47]	57.7 [46], [47]	2.67 [46], [47]	0.54 [46], [47]
ARF-CA	0.0112 mol resorcinol 0.0224 mol of 37% formaldehyde solution [43], [44], [45]	0.50 [43], [44], [45]	77 [43], [44], [45]	9.13 [43], [44], [45]	1000 [43], [44], [45]

2.2 Coating Aerogels with Collagen

Type I rat tail tendon collagen was obtained from Gibco and collagen solutions were prepared using 20 mM acetic acid solution. The collagen choice was based on successes in previous studies with aerogels, and, popularity of this type of collagen for developing biomedical implants and biomaterials [2], [54], [32]. The protocol used to coat the aerogel samples with collagen was based on successful procedures established in earlier studies [10], [11], [33], [48]. Briefly, aerogels were cut into coupons of approximately 0.5 x 0.5 x 0.2 cm^3 (w × l × h) which were fixed to the bottom of a petri dish with a clear adhesive sealant (Silicone RTV, Permatex) and allowed to cure

This journal is © The Royal Society of Chemistry 20xx

overnight. The exposed surface area of each aerogel coupon was measured carefully using the NIH open-source ImageJ (version 1.53t) software. This value was then used to calculate the amount of collagen solution needed to reach a final coating concentration ([c]) of 4, 8, 12, 16, or 20 μg/cm^2 [10, 11]. The starting collagen concentration was 4 μg/cm^2 which is the manufacturer's recommended concentration for PC 12 cells and was the baseline value for all our previous studies [13]. This concentration was incrementally increased by 2x, 3x, 4x, and 5x to determine the effect of collagen concentration on the architecture of the deposited collagen. Uncoated aerogels will be referred to as the "baseline" and microscopy glass slides coated with collagen will be referred to as the control.

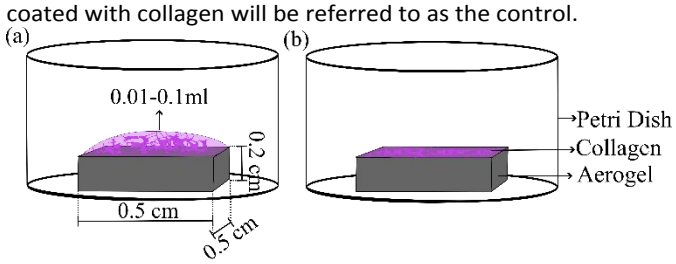

Figure 1. Schematic diagram of the deposition of collagen (purple) onto the upper surface of aerogel substrate (gray). (a) Collagen solution immediately after addition onto the aerogel substrate. (b) Remaining collagen layer after 1 hr. incubation and removal of the solution.

The aerogel-petri dish assembly was sterilized as previously described using a brief submersion in 100% ethanol followed by 20 min exposure to UV germicidal lamp (λ=254 nm) [9], [35]. The diluted collagen droplet was spread on the surface of interest until approximately 90% of the surface area was covered (Figure 1a). The petri dishes were then covered with a lid and the samples were incubated at room temperature for 1 hr to allow the deposition of collagen fibers onto the surface of the aerogel coupons. The left-over buffer from the collagen solution was gently washed with DI water and removed by careful aspiration with a micropipette (Elite, Fisher Scientific, Waltman, MA) taken care not to disturb the layer of deposited collagen (Figure 1b) [10], [35].

2.3 SEM Imaging

For SEM imaging, the aerogel with the deposited collagen layer was fixed with 2.5 % glutaraldehyde in 0.1 M sodium phosphate buffer (pH 7.4) [9-11] which was added dropwise onto the aerogel-petri dish combination that contained DI water. 1.5 ml was added gradually in 15 min. The diluted glutaraldehyde was then replaced with 2.5 % glutaraldehyde in 0.1 M sodium phosphate buffer fixation proceeded for 2 hrs at room temperature in a fume hood [10-11]. Next, 2×10 min washes with sodium phosphate buffer were performed. Samples were then dehydrated by a series of 1x10 min washes in 10%, 30%, 50%, 70%, 90%, and 100% ethanol [9], [35]. Samples were left to air dry before sputter coating (10 nm Au/Pd). Imaging was performed with a Scanning Electron Microscope (SEM) (Hitachi, Schaumburg, IL) [9], [34]. Figure 2 summarizes the steps mentioned above.

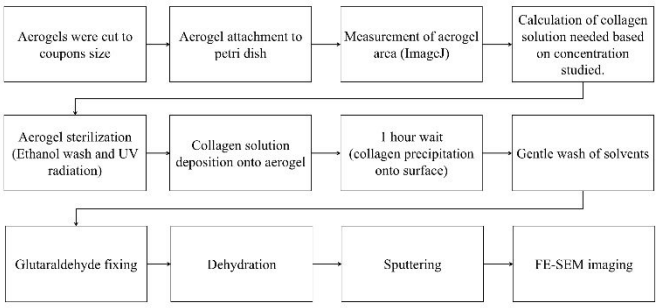

Figure 2. Flow diagram summarizing the sequence of steps involved in sample preparation.

Three independent trials (N = 3) were conducted for each type of aerogel and each collagen concentration. For the sake of consistency, the entire surface area of each sample was fully imaged and "sampled." To prevent any inconsistencies arising from unexpected and unintended sample curvature, only the central 5x5 grid area was utilized for calculations.

2.4 Immunofluorescence Microscopy

Aerogel coupons with 1x and 5x collagen densities were prepared as previously described as described above and fixed in 4% formaldehyde in phosphate buffered saline (PBS) for 15 min and washed with PBS (3 × 5 min) [49]. Aerogels were incubated for 30 min in a rabbit pro-collagen 1 polyclonal antibody (Bioss, Woburn, MA) diluted 1:100 in 1% BSA (Bovine serum albumin)/0.01 Tween-20 in PBS. After 3 × 5 min PBS washes to remove unbound primary antibodies, the coupons were incubated for 30 min with goat anti-rabbit IgGs conjugated to Alexa 488 and diluted 1:100 in 1% BSA (Bovine serum albumin)/0.01 Tween-20 in PBS. Unbound secondary antibodies were removed with 3 × 5 min PBS washes. The coupons were mounted with Prolong Diamond Antifade Mounting medium without DAPI (Thermofisher, Waltham, MA) onto the 14 mm glass coverslip of a 35 mm petri dish (MatTek, Ashland, MA). Finally, the mounting medium was allowed to cure overnight at 4 °C.

Microscopy observations of the distribution of collagen on aerogel substrates were performed with a confocal fluorescence laser scanning microscope (Nikon A1r, Tokyo, Japan). Observations were carried with a 20x objective and a pinhole size of 127.71. Z-stacked images were obtained over a depth of 50 μm and a Z-projection was performed with the image stack.

2.5 Image Analysis

SEM images were processed using the NIH open-source ImageJ (version 1.53t) software [50]. The scale was set using the scale bar of the SEM images. To facilitate the comparison of different images the field of view, magnification, and number of images per trial were kept the same for all samples imaged. Three parameters were used to quantify collagen deposition. These were (1) collagen fiber width (*w*), (2) collagen fiber length (*l*), and (3) areal coverage of collagen "films" whenever such films formed. Table 2 summarizes the different parameters used in this study, with symbols and definitions. Fibers were defined as filamentous structures which the length was at least three times

the width. Collagen fiber width (*w*) and length (*l*) were measured using the straight-line or segmented line tool (as appropriate) from ImageJ as schematized in Figure 3. For consistent measurements, fiber shape was approximated as a rectangular strip and fiber width (*w*) was measured only in the middle region of each fiber. Equation (1) below was used to calculate the total percentage areal coverage by the fibers (a_{fb}), assuming a 2D geometry:

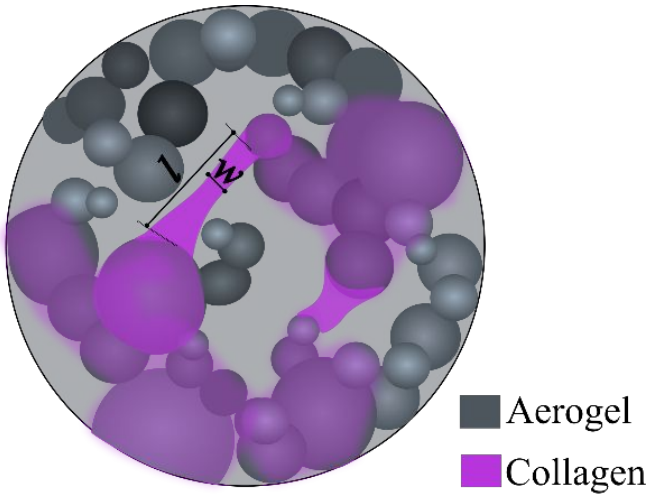

Figure 3. Schematic diagram showing how collagen fiber width and length were measured. A collagen fiber was defined as a filament for which the length (*l*) was at least three times the width (*w*). Collagen fiber width was measured at the middle of the fiber. From SEM images, collagen fiber width and length were measured using the straight-line or segmented line tool from ImageJ.

Table 2. Parameters used to characterize collagen fibers/films and aerogel substrates.

Symbol	Parameter	Description
w	Collagen fiber width (µm)	Normalized fiber width (normalized from 1x
l	Collagen fiber length (µm)	Normalized fiber length (normalized from 1x)
a_{fb}	Collagen Fiber area (%)	Percentage of surface area containing collagen in fiber form, compared to total area
a_{fm}	Collagen film surface (%)	Percentage of surface area containing collagen in a film form, compared to total area
[c]	Collagen surface density (note: concentration is ug/ml)	4 µg/cm², 8 µg/cm², 12 µg/cm², 16 µg/cm², or 20 µg/cm², labelled as 1x, 2x, 3x, 4x, or 5x, respectively
d	Aerogel pore diameter (µm)	Aerogel pore diameter
T.P.	Turning Point	Collagen concentration at which collagen appearance turns from fibers to film
Sa	Aerogel surface roughness (µm)	Arithmetic mean of the absolute distances of the surface points from the mean plane within a region of interest
Y	Aerogel Young's modulus (MPa)	Stiffness

$$a_{fb} = \frac{\sum_i^n w_i \cdot l_i}{Area_{field\ of\ view}} \times 100 \quad (1)$$

where w_i represents individual collagen fiber width, l_i represents individual fiber length, and $Area_{field\ of\ view}$ is the area of the field of view of the SEM image giving a percentage on the coverage of collagen fibers (a_{fb}).

The collagen layer was referred to as a "film" when an individual fiber was no longer discernible. Films were defined as a continuous collagen layer extending from one end of a pore to the opposite end such that the pore and/or pores underneath were masked. Areal coverage of the collagen film(s) (a_{fm}) was measured using the threshold tool in ImageJ providing a percentage of the film coverage of the overall field of view.

To describe the point at which the deposited collagen's appearance turned from fibers to a film, a new parameter, turning point (T.P.) was introduced. T.P. was defined for each aerogel type as the collagen concentration at which individual fibers were no longer distinguishable with the area covered by the film being >90% of the aerogel surface, or at which the area covered by fibers was less than 1% of the aerogel surface. The average of these values was used for calculating the final T.P.

2.6 Surface Roughness

Aerogels are inherently rough and non-uniform surfaces. The roughness can vary from nanometres to micrometres and depends on the aerogel type. Surface roughness measurements were obtained for control (glass slide), baseline (non-coated

This journal is © The Royal Society of Chemistry 20xx

aerogel), and collagen coated samples using a Profilm 3D (Filmetrics Inc. San Diego, CA) profilometer [9], [11], [34]. The surface area roughness was determined using the arithmetic mean height (*Sa*) over an area of 200 × 200 µm2 [10], [11], [34].

2.7 Collagen Thickness Measurement

The effect of collagen concentration on the thickness of deposited collagen was evaluated by two independent techniques: profilometry and microscopy. Microscope glass slides were coated with 1x-5x collagen concentrations, and an intentional straight-line scratch was introduced in the collagen layers with a sharp tipped spatula. The boundary between the glass and collagen was used to determine the thickness of the collagen layer, initially with the step height measurement profilometry technique and next confirming it using a SEM. The surface of the microscope slide was not scratched in this process.

2.8 Statistical Analysis

Statistical analysis was performed using Student's t-test with significance (*) defined as $p < 0.05$. For each collagen parameter measured (w, l, a_{fb}, a_{fm}), three independent trials (N = 3) were performed with 25 images (n = 25) acquired and analysed for each trial. Sa was measured in three independent trials (N = 3) within ten regions for each trial (n = 10). Error bars in the figures represent the standard error of the mean.

For profilometric collagen thickness measurements three independent experiments were used (N = 3) and for each trial the boundary between the collagen film and the glass slide was measured 10 times (n = 10) (at 10 different locations). Normalization to the 1x concentration was used to represent the increase in collagen thickness. The normalized values were compared to those obtained on SEM images using the same number of measurements.

3. Results and Discussion

3.1 Determining Collagen Layer Thickness

The thickness of collagen deposits was measured on a glass slide incubated with collagen concentrations ranging from 1x to 5x. This served as the control and helped us perfect the deposition technique. Thickness was normalized to the thickness of the collagen layer on slides incubated with 1x. The results indicate that the thickness of the deposited collagen layer increased linearly with increased collagen concentrations (Figure 4). This increase was modest as indicated the ~0.5 slope of line. Similar results were obtained when measurements were performed with two independent techniques, as mentioned in section 2.5. When the slides were incubated with collagen concentration >3x, the increase in thickness was marginal, which may be due to a tighter fiber packing density at high concentration.

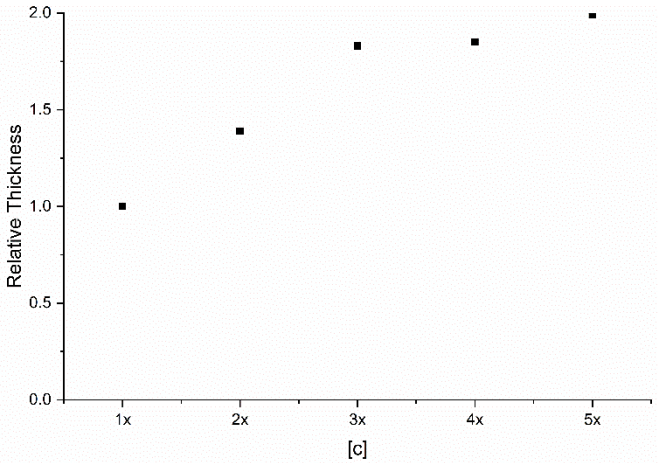

Figure 4. Normalized collagen thickness on glass coverslips as a function of the concentration of the collagen solution placed on the top surface of the aerogel; 1x-5x. Graph shows that the thickness of the collagen layer increases as the concentration increases.

3.2 The Morphology of the Collagen Layer Depends on the Concentration of Collagen in the Coating Solution

Here, we examined the effect of the collagen concentration in the incubation solution on the micromorphology of the collagen layer deposited onto various aerogels. Representative SEM images of control (glass) and each aerogel type (ARF-CA, Mix14, Mix18) incubated with at a 1x collagen concentration are shown in Figure 5. These observations demonstrated that the pore size influence the morphology of the collagen layer deposited. Upon increasing the collagen concentration in the

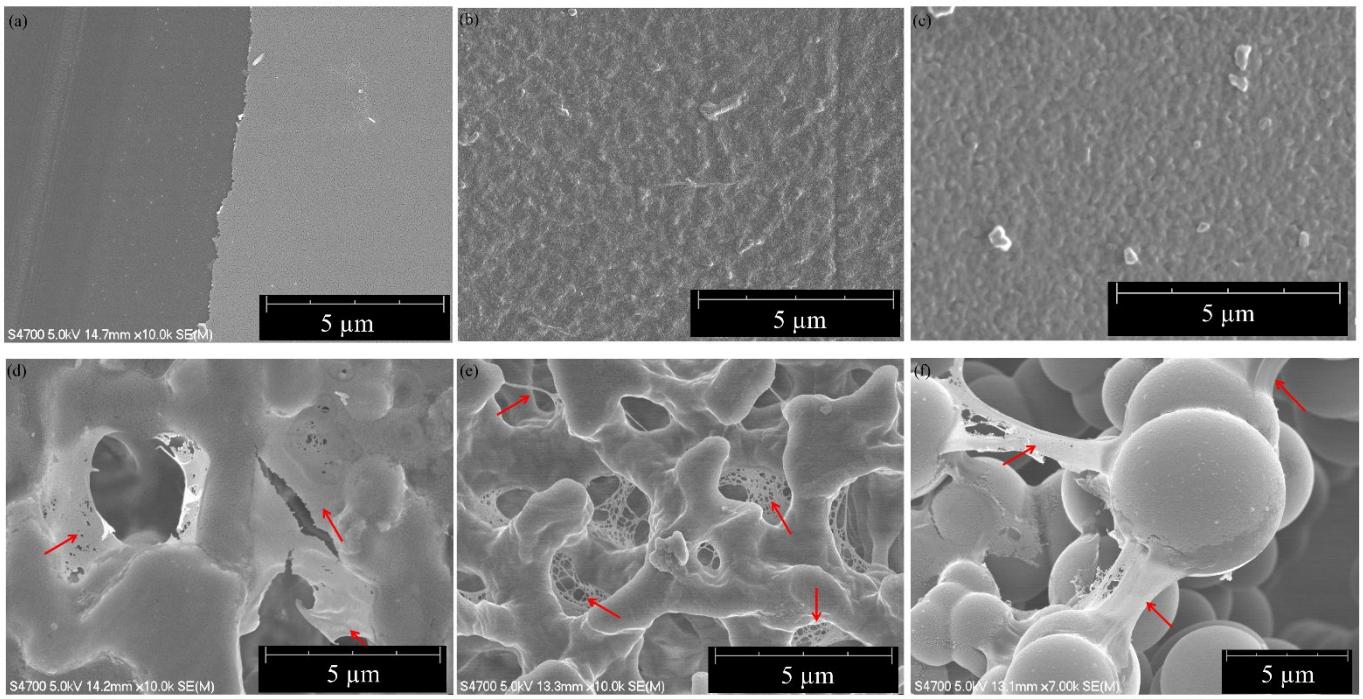

Figure 5. SEM images of the top surface of aerogels incubated with 1x collagen concentration on: (a) glass or control (left side: glass; right side: collagen layer), (b) PCSA, (c) BRF-CA, (d) Mix14, (e) Mix18, and (f) ARF-CA. Comparison between samples show the changes in collagen behavior in substrates of different pore diameters from thin films to fibers as the roughness and pore diameter of the aerogel increases.

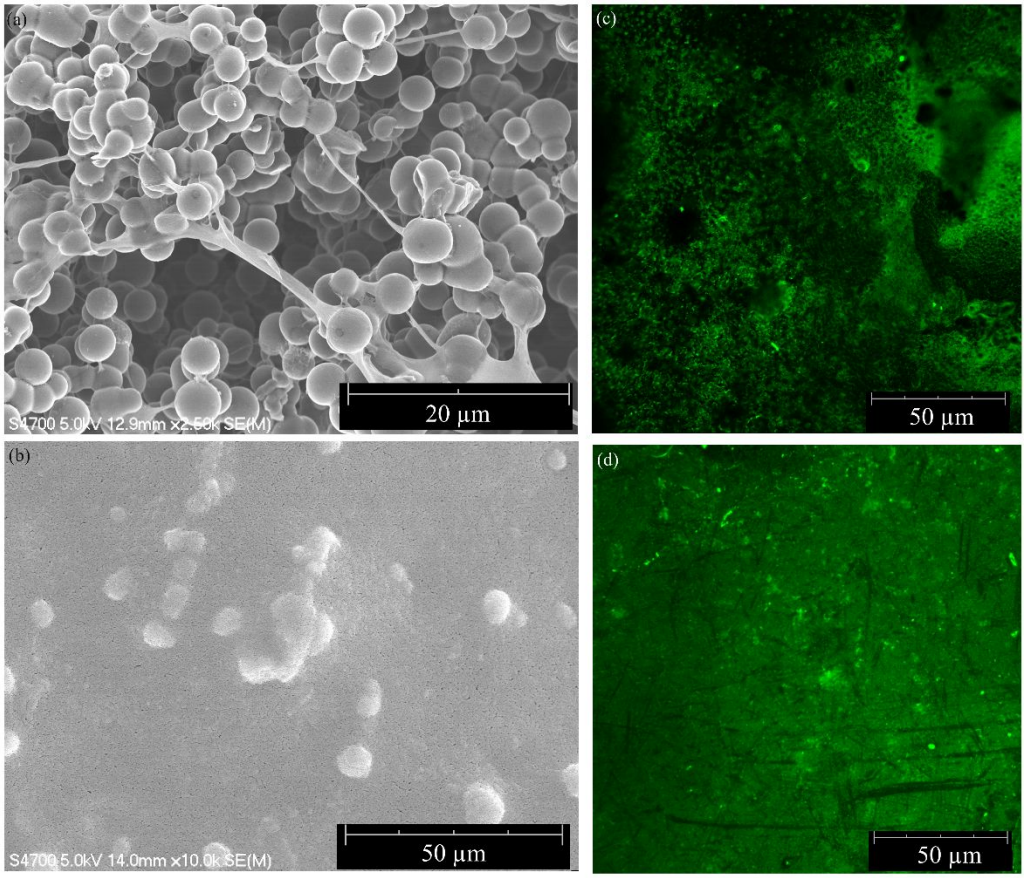

Figure 6. SEM (a, b) and confocal scanning fluorescence microscopy (c, d) images of the surface of ARF-CA onto which a 1x (a, b) or 5x (c, d) collagen solution has been deposited. For the fluorescence microscopy experiments, the ARF-CA surface was stained by immunofluorescence with collagen antibodies.

This journal is © The Royal Society of Chemistry 20xx

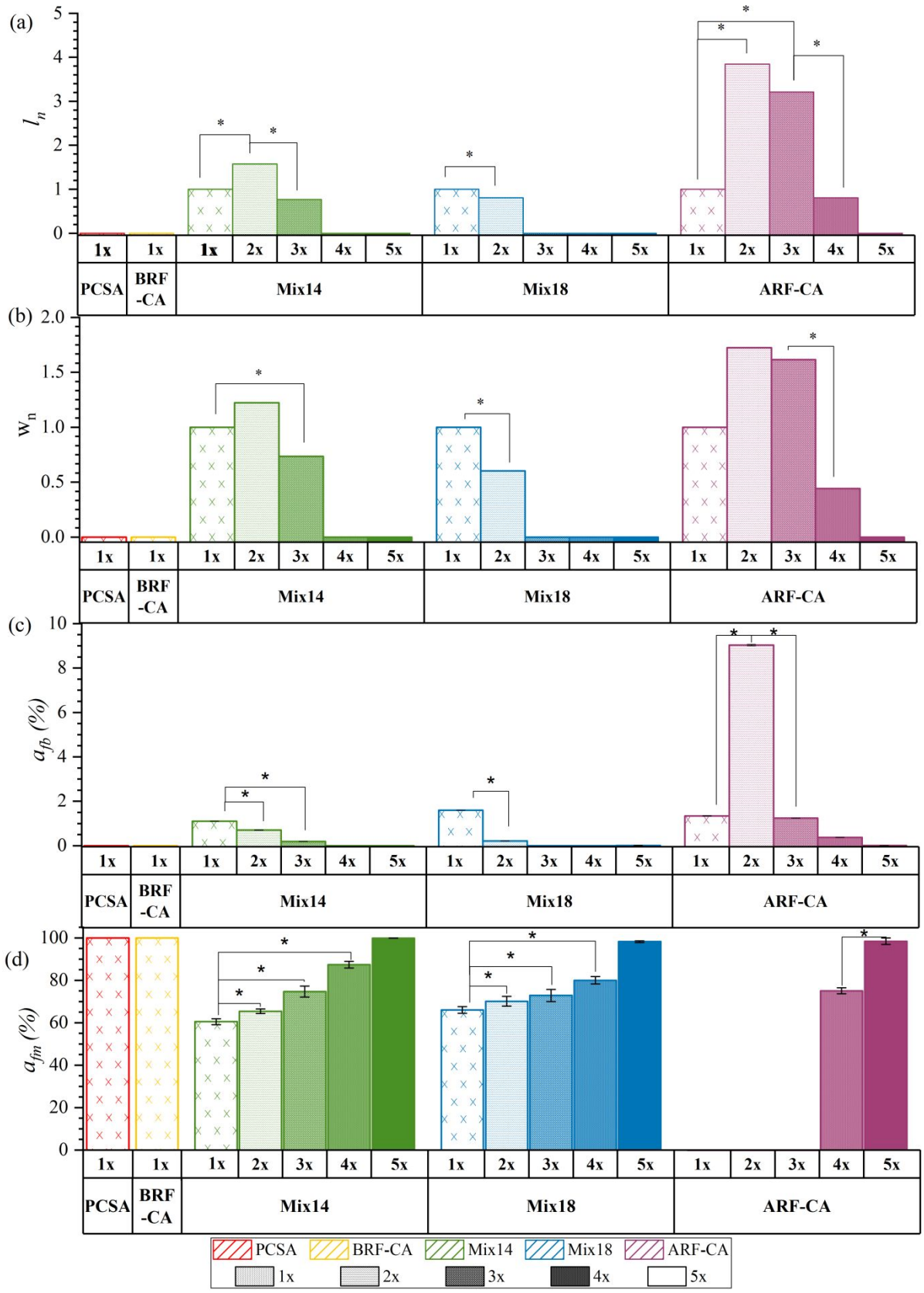

Figure 7. Behavior of collagen on different aerogel substrates. Normalized (a) fiber length (l_n) and (b) fiber width w_n,(c) percentage fiber area (a_{fb}) and (d) percentage film area (a_{fm}) of each aerogel type with increasing collagen concentration. X-axes show substrates with increasing pore diameter, and within each aerogel type, increasing collagen concentration. (*) shows statistical significance with p<0.05 using t-test. Normalized fiber length and fiber width increases with increasing collagen concentration until 2x, after which it decreases.

incubation solution, the morphology of the deposited collagen layer was either filamentous or formed a continuous sheet (film). Collagen fibers were conspicuous in ARF-CA (Figure 5f), as well as Mix18 aerogels (Figure 5e). As the collagen concentration in the incubation solution was increased, the fibrous appearance gradually turned into films covering the aerogel surface and masking the pores beneath it (Figure 6). Figures 6c and 6d are representative images of immunofluorescence staining for collagen which confirm that the surface covered with collagen in increased as the concentration of collagen in the incubation solution increased.

3.3 Non-linear Dependency of Collagen Fiber Length on Collagen Concentration

Two distinctly different collagen morphologies were observed and referred to as fibers and films. These were influenced by the pore diameter of the aerogel and by the concentration of collagen with which the aerogel was incubated. Figure 7 summarizes the morphology of the deposited collagen as a function of the pore diameter of the aerogel. Statistical significance (*) is shown using a t-test and a $p < 0.05$. For lower collagen concentrations (1x-3x), the deposited collagen formed fibers which length l_n and width w_n. were quantified [11]. Figure 7a shows the normalized length of collagen fibers for each aerogel type as a function of collagen concentration in the incubation solution. Films, but not fibers were observed in Mix14 at concentration higher than 4x and in Mix18 at concentration higher than 3x. l_n increased for collagen concentration lower than 3x. For 3x and above, l_n decreases as films were deposited instead of fibers.

Figure 7b shows the normalized w_n of collagen fibers on the different substrates. w_n increased for collagen concentration lower than 3x. For 3x and above, w_n decreases as films were deposited instead of fibers. Overall, a nonlinear relation was observed between collagen concentration and collagen fiber length and width.

3.4 Fiber to Film Transition Point

It was observed that the morphology of the collagen layer deposited gradually transitioned from filamentous to sheets as the collagen concentration in the incubation solution increased. Three parameters a_{fb}, a_{fm}, and T.P. were used to quantify and describe these changes. The percentage area covered by collagen fibers a_{fb} decreased with increasing collagen concentration (Figure 7c) as collagen fibers were replaced by collagen films. An exception to this trend was observed in ARF-CA incubated with 2x, with lead to a distinct increase in a_{fb}. Figure 7d shows an inverse trend compared to Figure 7c where a_{fm} increases with increasing collagen concentration. This is expected since the collagen transitions from fibers to films. In the case of ARF-CA, films were observed only at the highest concentrations (x4 and x5), while for both Mix14 and Mix18, films were observed for all concentrations due to higher Sa and d in ARF-CA compared to Mix14 and Mix18. To further highlight the effect of concentration on the appearance of the deposited collagen, l_n versus a_{fm} (Figure 8) shows an inverse relationship for all aerogel types.

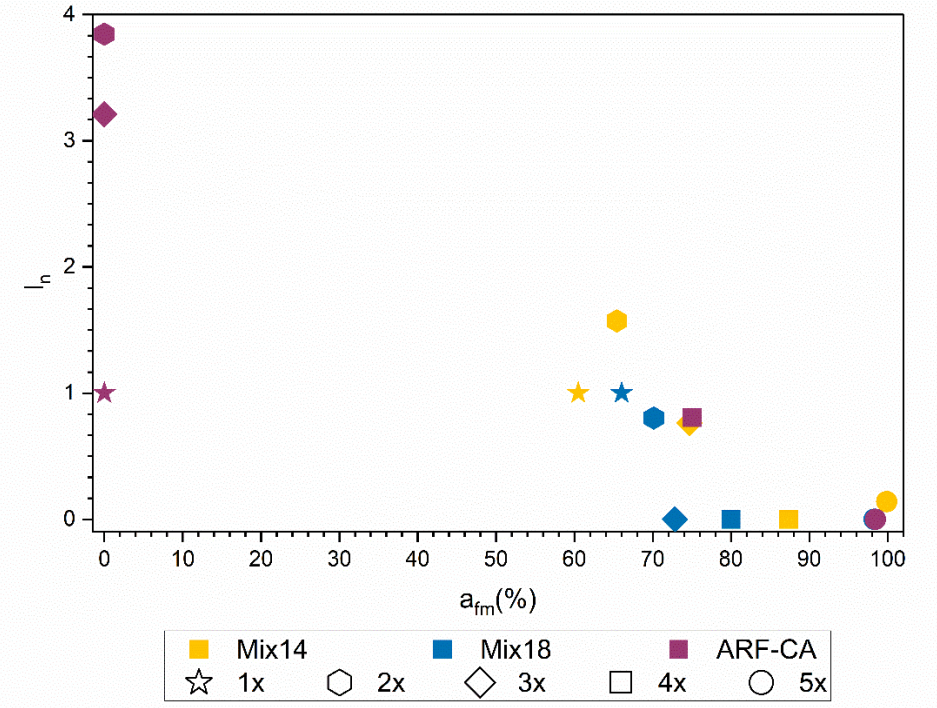

Figure 8: Dependency of normalized fiber length (l_n) on the percentage of the aerogel area covered by collagen films (a_{fm}) for Mix14, Mix18, and ARF-CA for collagen concentrations ranging from 1x to 5x). As the coverage increases the apparent fiber length decreases indicating a transition from a filamental appearance to a continuous film

This journal is © The Royal Society of Chemistry 20xx

Turning point (T.P.) was defined as the concentration at which fibers conjoin to form a film. Figure 9 shows the dependency of T.P. on *d, Y*, and *Sa* where T.P. is observed to increase with pore diameter, surface roughness, and stiffness for stiffness below 1 MPa. For Y values above 1 MPa, this trend does not continue and T.P. does not demonstrate a noticeable dependency on stiffness.

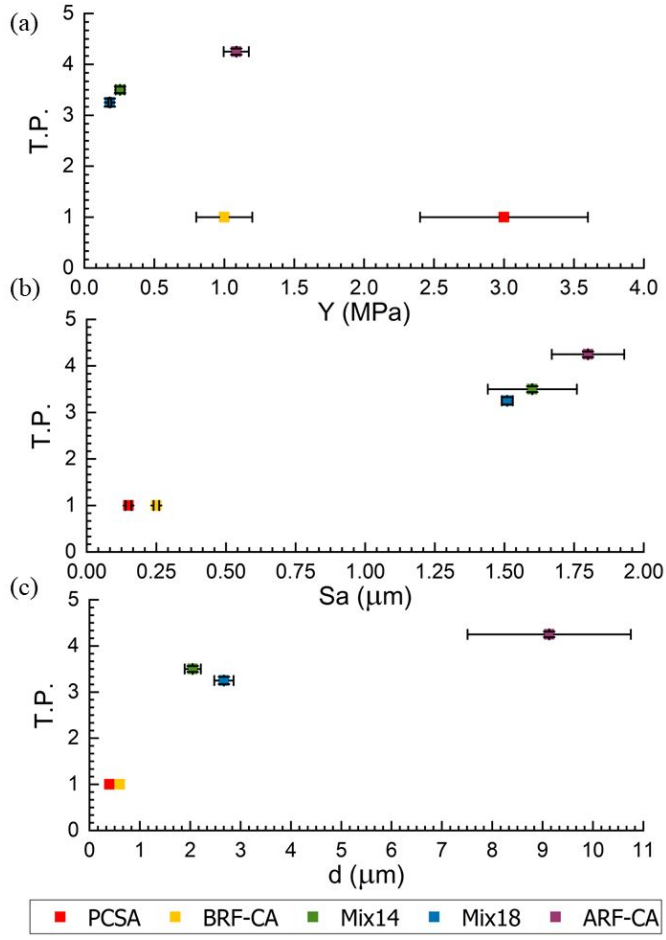

Figure 9: Dependency of T.P. on (a) Young's modulus (Y), (b) surface roughness (Sa), and (c) pore diameter (d) for all aerogels. In all cases T.P. increases with increasing d and Sa. However, T.P increases only for Mix-14, Mix18, and ARF-CA as the Young's modulus (Y) increases.

3.5 Increasing Collagen Concentration Masks Surface Roughness

Analysis of surface roughness (*Sa*) of each aerogel type with increasing collagen concentration was performed. Figure 10 shows 3D profile images of each aerogel type with increasing collagen concentration When Sa values were graphed against collagen concentration (Figure 11) an overall decrease in Sa was be observed for all aerogel types at concentrations >1x. This result is consistent with previous observations [11].

Further analysis of the different collagen parameters measured with surface roughness is shown in Figure 12 and include an overall decrease of a_{fm} with increasing *Sa* is observed (Figure 12a). As the concentration of collagen in the incubation solution increased from 1x to 5x, the aerogel area covered by collagen increased for all aerogels. The rate of this increase was dependent on the type of aerogel. As the film coverage increases, as expected, a_{fb} decreased for all aerogels (Figure 12b). For all aerogels examined, fiber width (w_n) appears to be independent of *Sa* prior to reaching the T.P. value (Figure 12c). Finally, ln displayed a nonlinear relationship with concentration, increasing first and then sharply decreasing because of the formation of films at higher concentrations (Figure 12d).

3.6 Experimental Approximation of Collagen Fibers Tension

Cell behavior such as proliferation, spreading, shape, and motility is affected by the mechanical properties of its microenvironment [51-54]. Collagen type I is the most prevalent component of the extracellular matrix (ECM) [2-4] and as such plays a critical role in the behavior of cells. When collagen is exposed to mechanical forces it can behave as an elastic, viscoelastic, or plastic [54-56]. When collagen filaments are under tension, the plastic nature of these fibers can lead to a "necking" effect which is directly correlated to the amount of tension experienced by the collagen fiber. In this study, such behavior was observed by SEM (Figures 13a and 13b). An important parameter that can be extracted from such observations is the amount of tension experienced by the collagen fiber, possibly due to its stretching across multiple pores. To calculate the tension, first, stress and strain had to be calculated using Equations 2 and 3. The stress and strain values were arrived at by focusing on the necking regions of the collagen fibers, caused by "strain softening" [56]. The parameters needed to complete this calculation were arrived at using Equations 4 and 5, as shown below:

$$strain = \Delta L / L_0 \quad (2)$$

$$stress = T/A \quad (3)$$

$$L_0 = L_1 + L_2 \quad (4)$$

$$A = \pi\left(\frac{W_n}{2}\right)^2 \quad (5)$$

where initial length of the collagen fiber is given by L_0, change in length by ΔL, and cross-sectional area by *A*. L_0 was calculated by measuring the length of the fibers in the regions that did not undergo necking, with consistent *w*. ΔL reflected the region of the fiber that did not undergo "necking". W_n however, was calculated from the width of the fiber in the neck region (Figure 13c)

Tension values calculated for 10 independent and randomly selected fibers are given in Table 3. The results show that there is no apparent correlation between pore diameter and fiber tension.

Our results suggest that for the parameter space we explored here, there is no dependency between pore diameter and tension in the collagen filament. Furthermore, "necking" was not observed in the regions covered with collagen films which can be explained by the fact that collagen in film form endures higher tension compared to fibers. This can be attributed to the stretch-dependent formation of weak cross-links that occur in collagen networks between fibers once stretched [54].

Figure 14 presents a schematic diagram depicting the geometric appearance of collagen on substrates with increasing *Sa*, as a function of concentration. When *Sa* is below 0.5 μm (left

column), the thickness of the collagen layer gradually increases, and it has a film-like appearance.

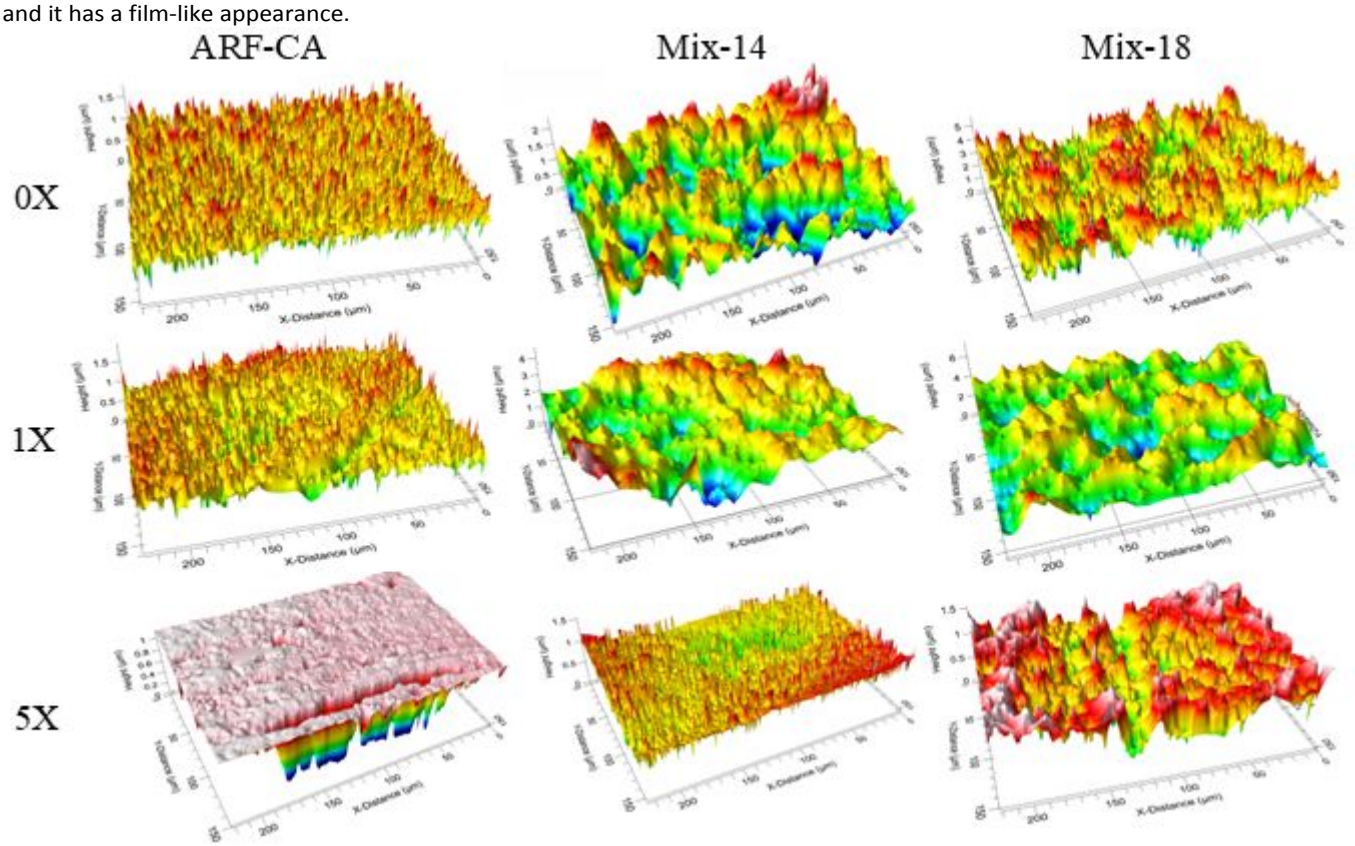

Figure 10. 3D profilometry view of aerogels ARF-CA (left column), Mix14 (middle column), and Mix18 (right column) coated with no collagen (upper row, baseline), 1x collagen (middle row) and 5x collagen (lower row). Within each column, the surface roughness decreases with increasing collagen concentration.

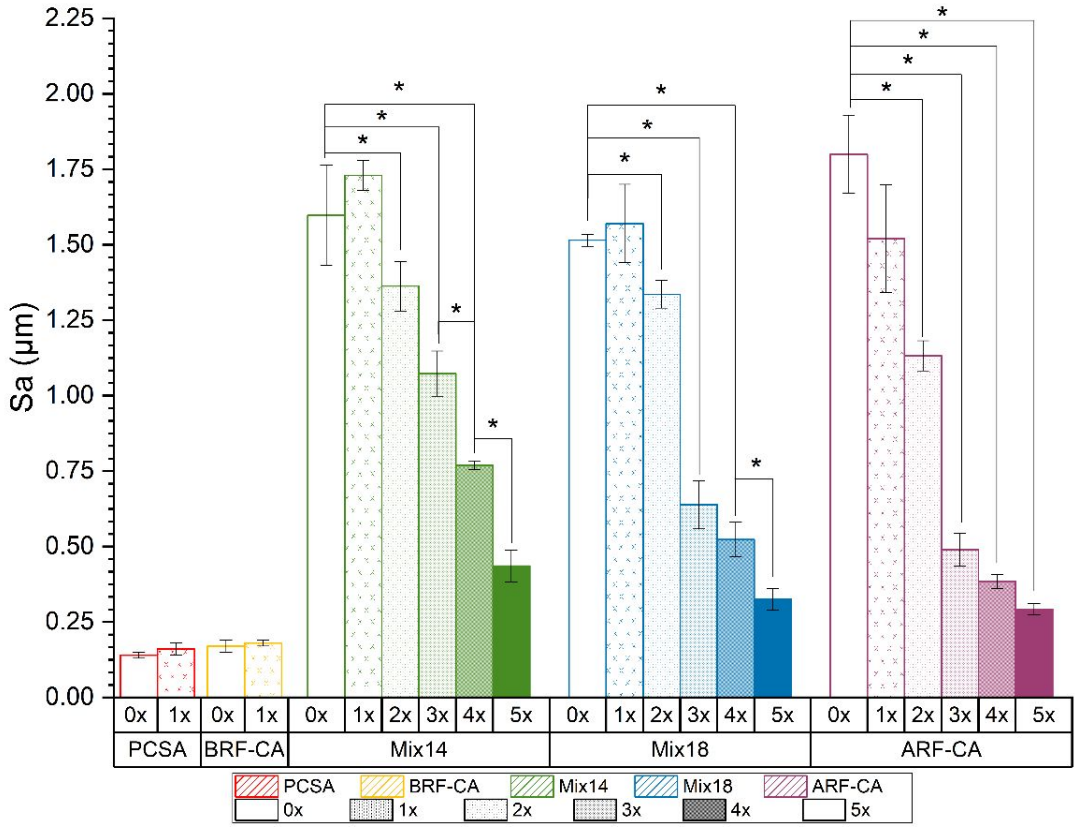

This journal is © The Royal Society of Chemistry 20xx

Figure 11. Surface roughness (Sa) of each aerogel type (PCSA, BRF-CA, Mix14, Mix18 and ARF-CA) incubated with increasing collagen concentration (0x-5x). Changes in Sa between 0x and 1x are not significant. When concentrations of collagen greater than 1x are compared to each other, there is a progressively more pronounced and statistically significant decrease in Sa.

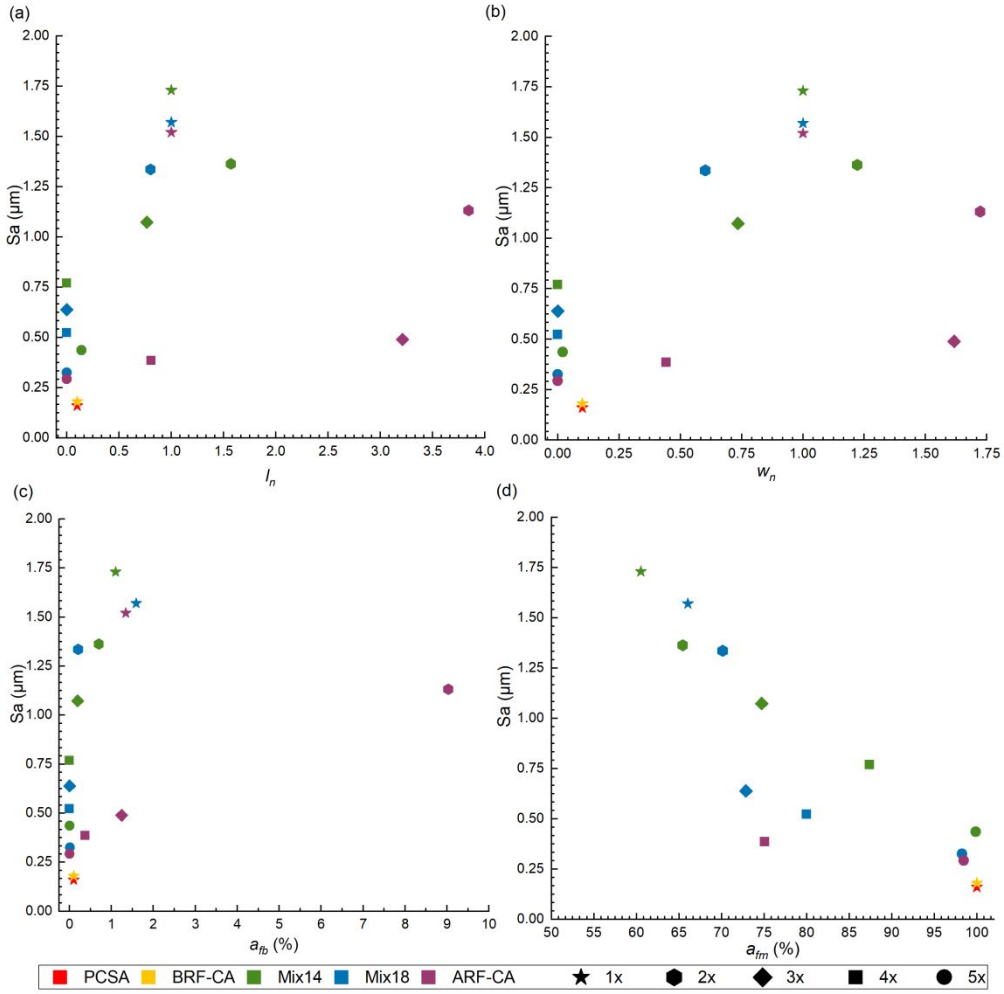

Figure 12: Surface roughness as a function of (a) percentage fiber area (a_{fb}), (b) percentage film area (a_{fm}), (c) normalized fiber width (w_n), and (d) normalized fiber length (l_n) for each aerogel substrate and with increasing collagen concentration.

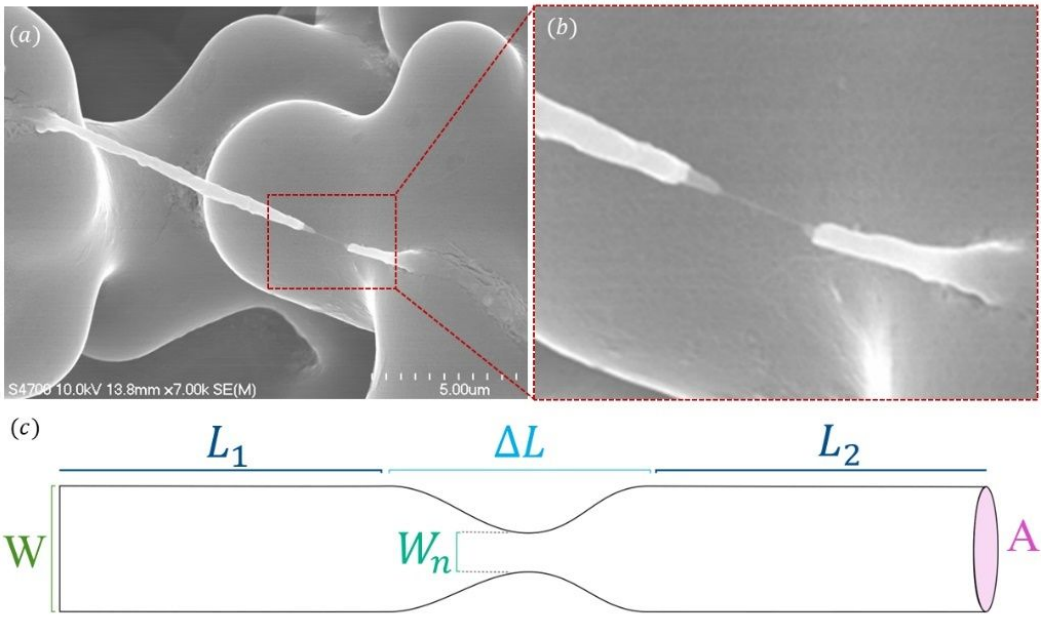

Figure 13: Role of tension in collagen fibers: (a) SEM image of collagen fiber on ARF-CA, where the change in width of fiber can be easily observed. (b) Augmented SEM image for further detail observation. (c) Schematic diagram of the parameters used to calculate tension based on change in width of collagen fibers.

This journal is © The Royal Society of Chemistry 20xx

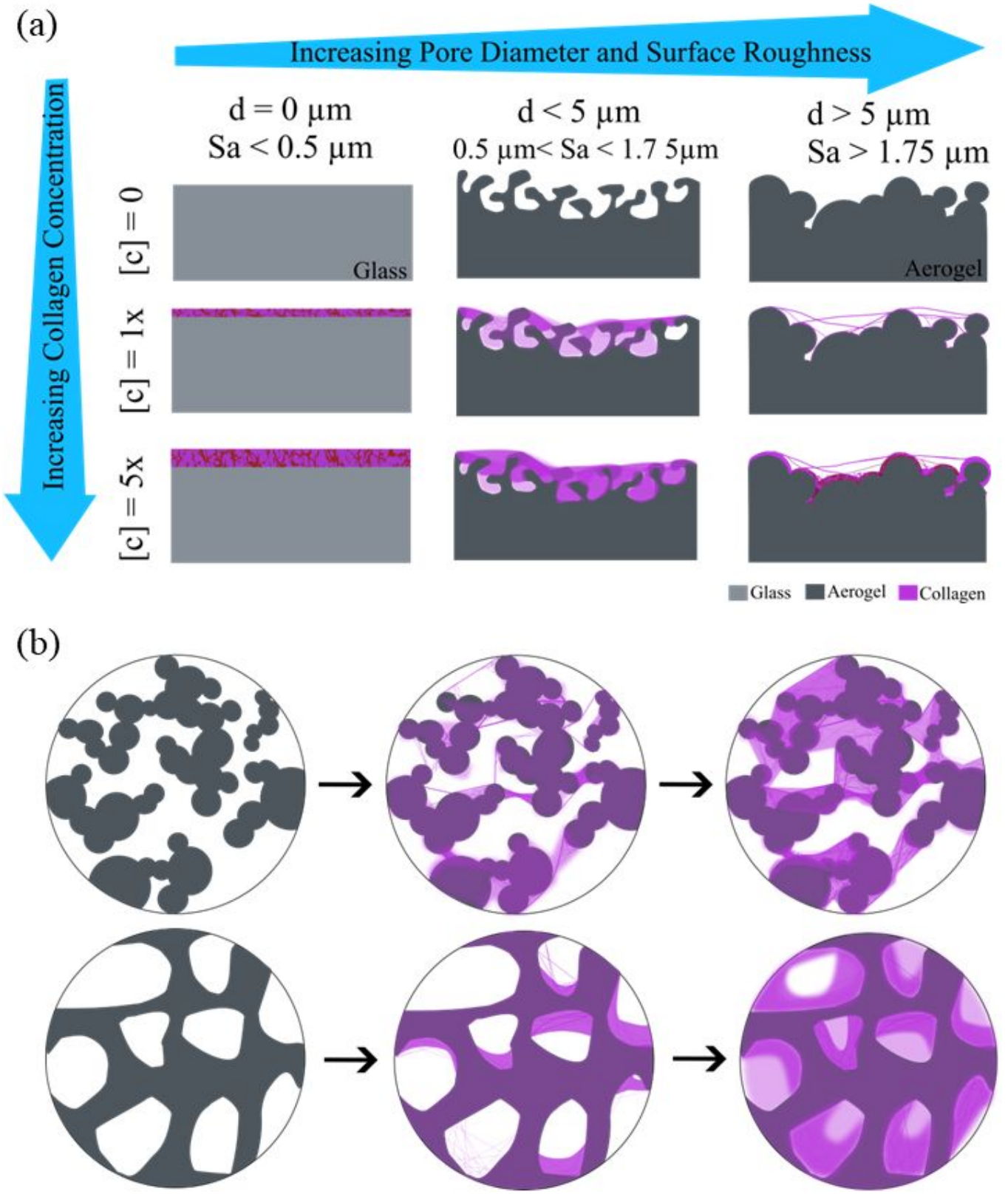

Figure 14. Schematic diagrams modelling collagen deposition on substrates and collagen behavior based on different surface topography and pore diameter. The behavior transitions from filaments to film as substrate properties and coating concentration changes.

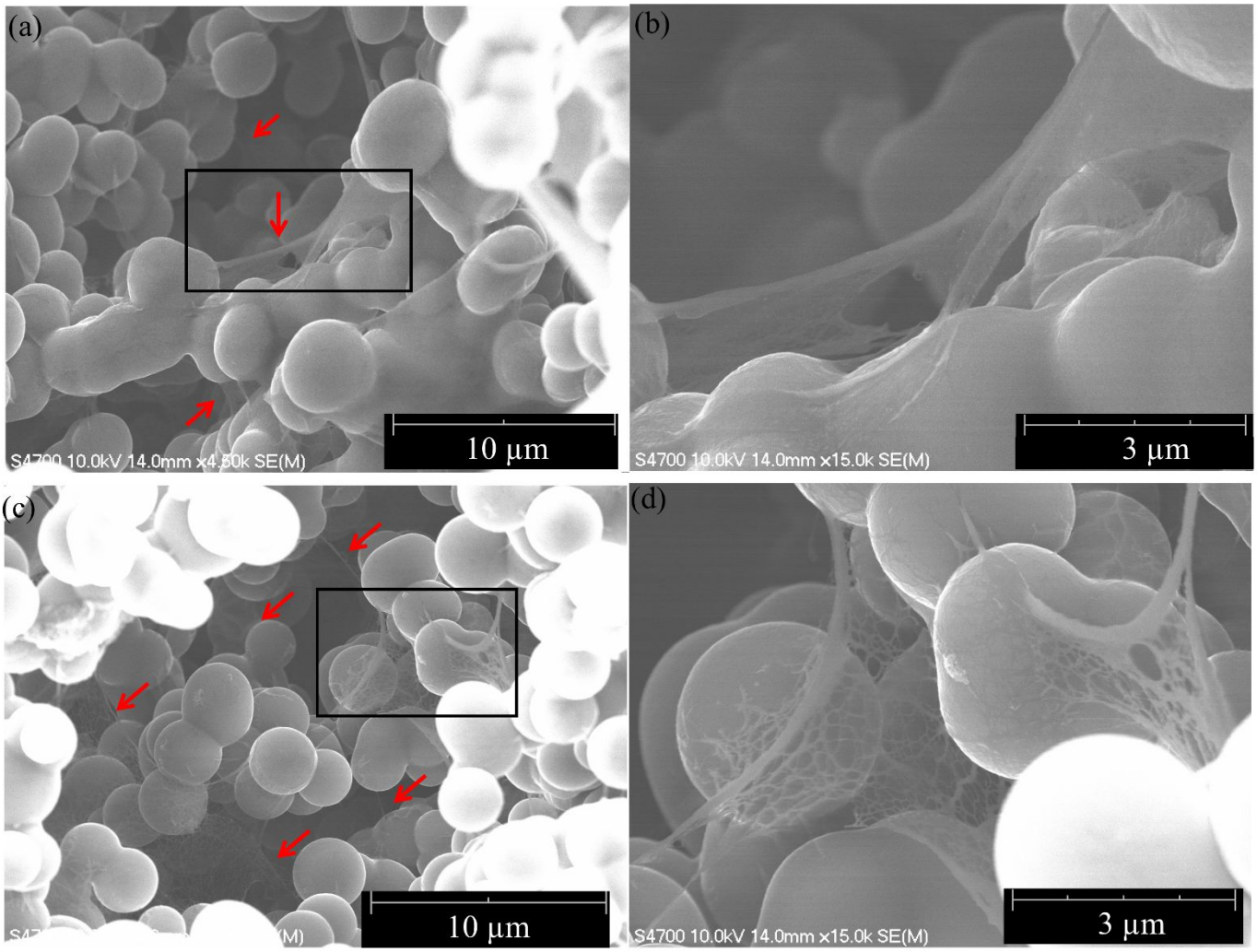

Figure 15. SEM image of ARF-CA after incubation with 2x collagen solution demonstrating the presence of collagen fibers deep within the pores. Red arrows in (a) and (c) point at collagen fibers. (b) and (d) show a higher magnification of the inset in (a) and (c), respectively. Images demonstrate that some collagen fibers are embedded deep within the bulk of the aerogels with a pore diameter larger than 5 µm.

When 1 µm < *Sa* < 1.75 µm (middle column), the collagen layer develops a film-like appearance at a higher concentration than noted earlier. At the onset of the film appearance, individual fibers and films are both present (Figure 14-a5). For Sa values greater than 1.75 µm (right column), both fibers and film are present at the highest concentration (Figure 14-a9). This information is valuable for customization and tailoring of biomaterials since the collagen appearance can be easily manipulated to fit the desired topography. To further demonstrate the collagen-aerogel interaction, a top view of schematic diagram is given in Figure 14b

The transformation of collagen from fibers to film and the respective areal coverage (a_{fb} and a_{fm}) in each case was described in Figures 7c and 7d. While it is reasonable to expect these two parameters to complement one another, in some cases and particularly for aerogels with d > 5um, it does not occur in practice. We attribute this discrepancy to collagen fibers entering the pores of some of the aerogels as can be seen in Figure 15. The missing portion is buried within the bulk of the aerogel.

Table 3. Summary of tension in fibers as a function of pore diameter.

Fiber #	Pore Diameter (µm)	Tension (N)
1	2.03 ± 0.01	$1.4 \times 10^{-12} \pm 9 \times 10^{-9}$
2	2.40 ± 0.01	$1.92 \times 10^{-12} \pm 9 \times 10^{-9}$
3	2.66 ± 0.01	$5.20 \times 10^{-13} \pm 9 \times 10^{-9}$
4	2.90 ± 0.01	$1.8 \times 10^{-12} \pm 9 \times 10^{-9}$
5	4.04 ± 0.01	$1.84 \times 10^{-12} \pm 9 \times 10^{-9}$
6	4.64 ± 0.01	$8.02 \times 10^{-12} \pm 9 \times 10^{-9}$
7	4.74 ± 0.01	$3.25 \times 10^{-12} \pm 9 \times 10^{-9}$
8	4.83 ± 0.01	$2.49 \times 10^{-12} \pm 9 \times 10^{-9}$
9	6.71 ± 0.01	$1.47 \times 10^{-12} \pm 9 \times 10^{-9}$
10	11.79 ± 0.01	$4.68 \times 10^{-12} \pm 9 \times 10^{-9}$

Conclusions

A basic understanding of the influence of surface topography on collagen deposition is important for designing collagen-coated materials for biomedical applications. In this study, we have characterized the effect of topography and stiffness of five

This journal is © The Royal Society of Chemistry 20xx

different aerogel substrates on the structural features of collagen deposits. The key conclusions from this study are:

1. The architecture of collagen deposits transitions from discrete (individual fibers) to continuous (film-like) as a function of both collagen concentration and surface characteristics of the aerogels. With the turning point (T.P.) being defined as the collagen concentration at which this transition occurs, we show that T.P. increases with increasing surface roughness and pore diameter. This emphasizes the importance of the surface topography of the substrate for the structure of collagen deposits [42], [57], [58]. Young's modulus, however, only modestly affects T.P.
2. At concentrations of collagen inferior to T.P., the length and width of collagen fibers are determined by the aerogel pore diameter such that the greater the pore diameter, the larger the fiber length and fiber width.
3. Data suggests that for aerogels with pore diameters greater than 5 μm, a certain volume of the deposited collagen is not confined to the surface but enters the pores and therefore does not contribute to the collagen profile observed superficially (Figure 7c-7d).
4. At concentrations of collagen inferior to T.P., collagen deposition did not affect the surface roughness of aerogels (Figure 11). However, at concentrations higher than T.P. the aerogel surface topography was gradually masked by the collagen film.

In conclusion, cellular behavior during wound healing and nerve repair depends on a multiplicity of factors including surface topography and the type of proteins coating the substrate. Here, we demonstrate for collagen that the structural features of the protein deposited on the substrate are also affected by the substrate surface topography. In the case of collagen, it is possible to choose configurations of substrate topography and collagen concentrations that will result in fibrous or continuous coating. It remains to be examined which of these structural features is optimal for wound healing and nerve repair.

Author contributions

MRS: Methodology, Data curation, Investigation, writing original draft and editing. OS: Resources, Writing – review and editing, Investigation. SC: Resources, Writing – review and editing. NL: Resources, Writing – review and editing. MW: Resources, Writing – review and editing. FS: Conceptualization, Formal analysis, Funding acquisition, Investigation, Methodology, Project administration, Supervision, Validation, Visualization, Writing – original draft, revision, editing

Conflicts of interest

There are no conflicts to declare.

Data availability

There are no conflicts to declare.

Acknowledgements

Author Firouzeh Sabri was supported under NSF Award # 1852549. We would like to also acknowledge Autumn Jones for assistance with project. Authors Swetha Chandraskaran and Marcus Worsley was supported by Lawrence Livermore National Laboratory under the auspices of the U.S. Department of Energy (No. DE-AC52-07NA27344).

References

1 I. N. Amirrah, Y. Lokanathan, I. Zulkiflee, M. F. M. R. Wee, A. Motta, and M. B. Fauzi, "A Comprehensive Review on Collagen Type I Development of Biomaterials for Tissue Engineering: From Biosynthesis to Bioscaffold," Biomedicines, vol. 10, no. 9, p. 2307, Sep. 2022, doi: 10.3390/biomedicines10092307.
2 M. D. Shoulders and R. T. Raines, "Collagen structure and stability.," Annu Rev Biochem, vol. 78, pp. 929–58, 2009, doi: 10.1146/annurev.biochem.77.032207.120833.
3 A. Sorushanova et al., "The Collagen Suprafamily: From Biosynthesis to Advanced Biomaterial Development.," Advanced materials, vol. 31, no. 1, p. e1801651, Jan. 2019, doi: 10.1002/adma.201801651.
4 B. Sun, "The mechanics of fibrillar collagen extracellular matrix," Cell Rep Phys Sci, vol. 2, no. 8, p. 100515, Aug. 2021, doi: 10.1016/j.xcrp.2021.100515.
5 K. Henriksen and M. A. Karsdal, "Type I Collagen," in Biochemistry of Collagens, Laminins and Elastin, Elsevier, 2016, pp. 1–11. doi: 10.1016/B978-0-12-809847-9.00001-5.
6 H. A. B. Multhaupt, B. Leitinger, D. Gullberg, and J. R. Couchman, "Extracellular matrix component signaling in cancer," Adv Drug Deliv Rev, vol. 97, pp. 28–40, Feb. 2016, doi: 10.1016/j.addr.2015.10.013.
7 R. W. Farndale et al., "Cell–collagen interactions: the use of peptide Toolkits to investigate collagen–receptor interactions," Biochem Soc Trans, vol. 36, no. 2, pp. 241–250, Apr. 2008, doi: 10.1042/BST0360241.
8 L. A. Greene and A. S. Tischler, "Establishment of a noradrenergic clonal line of rat adrenal pheochromocytoma cells which respond to nerve growth factor.," Proceedings of the National Academy of Sciences, vol. 73, no. 7, pp. 2424–2428, 1976, doi: 10.1073/pnas.73.7.2424.
9 M. Rodriguez Sala, K. J. Lynch, S. Chandrasekaran, O. Skalli, M. Worsley, and F. Sabri, "PC-12 cells adhesion and differentiation on carbon aerogel scaffolds," MRS Commun, vol. 8, no. 4, 2018, doi: 10.1557/mrc.2018.206.
10 M. Rodriguez Sala, S. Chandrasekaran, O. Skalli, M. Worsley, and F. Sabri, "Enhanced neurite outgrowth on electrically conductive carbon aerogel substrates in the presence of an external electric field," Soft Matter, vol. 17, no. 17, pp. 4489–4495, 2021, doi: 10.1039/D1SM00183C.
11 M. R. Sala, O. Skalli, and F. Sabri, "Optimal structural and physical properties of aerogels for promoting robust neurite extension in vitro," Biomaterials Advances, vol. 135, p. 112682, 2022, doi: https://doi.org/10.1016/j.msec.2022.112682.
12 K. J. Lynch, O. Skalli, and F. Sabri, "Investigation of surface topography and stiffness on adhesion and neurites extension of PC12 cells on crosslinked silica aerogel substrates," PLoS One, vol. 12, no. 10, Oct. 2017, doi: 10.1371/journal.pone.0185978.

13 L. A. Greene, J. M. Aletta, A. Rukenstein, and S. H. Green, "[18] PC12 pheochromocytoma cells: culture, nerve growth factor treatment, and experimental exploitation," Methods Enzymol, vol. 147, no. C, pp. 207–216, Jan. 1987, doi: 10.1016/0076-6879(87)47111-5.
14 X. Wang, T. Lou, W. Zhao, G. Song, C. Li, and G. Cui, "The effect of fiber size and pore size on cell proliferation and infiltration in PLLA scaffolds on bone tissue engineering," J Biomater Appl, vol. 30, no. 10, pp. 1545–1551, May 2016, doi: 10.1177/0885328216636320.
15 P. Joly et al., "Geometry-Driven Cell Organization Determines Tissue Growths in Scaffold Pores: Consequences for Fibronectin Organization," PLoS One, vol. 8, no. 9, p. e73545, Sep. 2013, doi: 10.1371/journal.pone.0073545.
16 A. D. Doyle and K. M. Yamada, "Mechanosensing via cell-matrix adhesions in 3D microenvironments," Exp Cell Res, vol. 343, no. 1, pp. 60–66, Apr. 2016, doi: 10.1016/j.yexcr.2015.10.033.
17 M. K. Lee, M. H. Rich, J. Lee, and H. Kong, "A bio-inspired, microchanneled hydrogel with controlled spacing of cell adhesion ligands regulates 3D spatial organization of cells and tissue," Biomaterials, vol. 58, pp. 26–34, Jul. 2015, doi: 10.1016/j.biomaterials.2015.04.014.
18 K. Wolf et al., "Collagen-based cell migration models in vitro and in vivo," Semin Cell Dev Biol, vol. 20, no. 8, pp. 931–941, Oct. 2009, doi: 10.1016/j.semcdb.2009.08.005.
19 C. N. Grover, R. E. Cameron, and S. M. Best, "Investigating the morphological, mechanical and degradation properties of scaffolds comprising collagen, gelatin and elastin for use in soft tissue engineering," J Mech Behav Biomed Mater, vol. 10, pp. 62–74, Jun. 2012, doi: 10.1016/j.jmbbm.2012.02.028.
20 C. H. Lee, A. Singla, and Y. Lee, "Biomedical applications of collagen," Int J Pharm, vol. 221, no. 1, pp. 1–22, 2001, doi: https://doi.org/10.1016/S0378-5173(01)00691-3.
21 S. Zhang et al., "Bi-layer collagen/microporous electrospun nanofiber scaffold improves the osteochondral regeneration," Acta Biomater, vol. 9, no. 7, pp. 7236–7247, Jul. 2013, doi: 10.1016/j.actbio.2013.04.003.
22 "Control of Cell Behavior: Topological Factors," JNCI: Journal of the National Cancer Institute, Jul. 1964, doi: 10.1093/jnci/33.1.15.
23 K. Sheets, S. Wunsch, C. Ng, and A. S. Nain, "Shape-dependent cell migration and focal adhesion organization on suspended and aligned nanofiber scaffolds," Acta Biomater, vol. 9, no. 7, pp. 7169–7177, Jul. 2013, doi: 10.1016/j.actbio.2013.03.042.
24 T. Ferreira-Gonçalves, C. Constantin, M. Neagu, C. P. Reis, F. Sabri, and R. Simón-Vázquez, "Safety and efficacy assessment of aerogels for biomedical applications," Biomedicine and Pharmacotherapy, vol. 144, Dec. 2021, doi: 10.1016/j.biopha.2021.112356.
25 N. Mansouri and SamiraBagheri, "The influence of topography on tissue engineering perspective," Materials Science and Engineering: C, vol. 61, pp. 906–921, Apr. 2016, doi: 10.1016/j.msec.2015.12.094.
26 J. J. Norman and T. A. Desai, "Methods for Fabrication of Nanoscale Topography for Tissue Engineering Scaffolds," Ann Biomed Eng, vol. 34, no. 1, pp. 89–101, Mar. 2006, doi: 10.1007/s10439-005-9005-4.
27 F. Sabri, K. J. Lynch, and S. Allison, "Polymer-encapsulated phosphor particles for in vivo phosphor luminescence applications," International Journal of Polymeric Materials and Polymeric Biomaterials, vol. 64, no. 13, pp. 690–694, Nov. 2015, doi: 10.1080/00914037.2014.1002096.
28 F. Sabri, J. A. Cole, M. C. Scarbrough, and N. Leventis, "Investigation of polyurea-crosslinked silica aerogels as a neuronal scaffold: A pilot study," PLoS One, vol. 7, no. 3, Mar. 2012, doi: 10.1371/journal.pone.0033242.
29 S. W. Allison, E. S. Baker, K. J. Lynch, and F. Sabri, "In Vivo X-Ray Imaging of Phosphor-Doped PDMS and Phosphor-Doped Aerogel Biomaterials," International Journal of Polymeric Materials and Polymeric Biomaterials, vol. 64, no. 16, pp. 823–830, Dec. 2015, doi: 10.1080/00914037.2015.1030652.
30 F. Sabri, M. E. Sebelik, R. Meacham, J. D. Boughter, M. J. Challis, and N. Leventis, "In Vivo Ultrasonic Detection of Polyurea Crosslinked Silica Aerogel Implants," PLoS One, vol. 8, no. 6, Jun. 2013, doi: 10.1371/journal.pone.0066348.
31 F. Sabri et al., "Histological Evaluation of the Biocompatibility of Polyurea Crosslinked Silica Aerogel Implants in a Rat Model: A Pilot Study," PLoS One, vol. 7, no. 12, Dec. 2012, doi: 10.1371/journal.pone.0050686.
32 F. Sabri, D. Gerth, G.-R. M. Tamula, T.-C. N. Phung, K. J. Lynch, and J. D. Boughter Jr, "Novel Technique for Repair of Severed Peripheral Nerves in Rats Using Polyurea Crosslinked Silica Aerogel Scaffold," Journal of Investigative Surgery, vol. 27, no. 5, pp. 294–303, Oct. 2014, doi: 10.3109/08941939.2014.906688.
33 K. Lynch, O. Skalli, and F. Sabri, "Growing Neural PC-12 Cell on Crosslinked Silica Aerogels Increases Neurite Extension in the Presence of an Electric Field," J Funct Biomater, vol. 9, no. 2, p. 30, Apr. 2018, doi: 10.3390/jfb9020030.
34 M. R. Sala, O. Skalli, N. Leventis, and F. Sabri, "Nerve response to superelastic shape memory polyurethane aerogels," Polymers (Basel), vol. 12, no. 12, 2020, doi: 10.3390/polym12122995.
35 M. Rodriguez Sala, C. Peng, O. Skalli, and F. Sabri, "Tunable neuronal scaffold biomaterials through plasmonic photo-patterning of aerogels," MRS Commun, vol. 9, no. 4, pp. 1249–1255, 2019, doi: 10.1557/mrc.2019.143.
36 M. Rodriguez Sala, S. Ghimire, G. Raptopoulos, P. Paraskevopoulou, and F. Sabri, "Investigation and characterization of time-dependent degradation of X-Ca-alginate aerogels for biomedical applications," J Mater Sci, vol. 58, no. 30, pp. 12331–12350, Aug. 2023, doi: 10.1007/s10853-023-08778-9.
37 S. Ghimire et al., "Noninvasive Detection, Tracking, and Characterization of Aerogel Implants Using Diagnostic Ultrasound," Polymers, vol. 14, no. 4, p. 722, 2022, doi: 10.3390/polym14040722.
38 S. Ghimire and F. Sabri, "K-wave modelling of ultrasound wave propagation in aerogels and the effect of physical parameters on attenuation and loss," Applied Physics A, vol. 129, no. 4, p. 286, Apr. 2023, doi: 10.1007/s00339-023-06586-1.
39 S. W. Allison, E. S. Baker, K. J. Lynch, and F. Sabri, "In vivo X-Ray excited optical luminescence from phosphor-doped aerogel and Sylgard 184 composites," Radiation Physics and Chemistry, vol. 135, pp. 88–93, 2017, doi: https://doi.org/10.1016/j.radphyschem.2017.01.045.
40 P. Paraskevopoulou et al., "Polyurea-crosslinked biopolymer aerogel beads," RSC Adv., vol. 10, no. 67, pp. 40843–40852, 2020, doi: 10.1039/D0RA07337G.
41 P. Paraskevopoulou et al., "Mechanically Strong Polyurea/Polyurethane-Cross-Linked Alginate Aerogels," ACS Appl Polym Mater, vol. 2, no. 5, pp. 1974–1988, 2020, doi: 10.1021/acsapm.0c00162.
42 G. Lai, Y. Li, and G. Li, "Effect of concentration and temperature on the rheological behavior of collagen solution," Int J Biol Macromol, vol. 42, no. 3, pp. 285–291, Apr. 2008, doi: 10.1016/j.ijbiomac.2007.12.010.
43 T. F. Worsley Marcus A. and Baumann, "Carbon Aerogels," in Handbook of Sol-Gel Science and Technology, M. and J. A. Klein Lisa and Aparicio, Ed., Cham: Springer International Publishing, 2016, pp. 1–36. doi: 10.1007/978-3-319-19454-7_90-1.
44 S. Chandrasekaran, P. G. Campbell, T. F. Baumann, and M. A. Worsley, "Carbon aerogel evolution: Allotrope, graphene-

 This journal is © The Royal Society of Chemistry 20xx

inspired, and 3D-printed aerogels," J Mater Res, vol. 32, no. 22, pp. 4166–4185, 2017, doi: 10.1557/jmr.2017.411.
45 M. A. Worsley, J. H. Satcher, and T. F. Baumann, "Synthesis and characterization of monolithic carbon aerogel nanocomposites containing double-walled carbon nanotubes," Langmuir, vol. 24, no. 17, pp. 9763–9766, Sep. 2008, doi: 10.1021/la8011684.
46 S. Donthula et al., "Nanostructure-Dependent Marcus-Type Correlation of the Shape Recovery Rate and the Young's Modulus in Shape Memory Polymer Aerogels," ACS Appl Mater Interfaces, vol. 10, no. 27, pp. 23321–23334, Jul. 2018, doi: 10.1021/acsami.8b06234.
47 S. Donthula et al., "Shape Memory Superelastic Poly(isocyanurate-urethane) Aerogels (PIR-PUR) for Deployable Panels and Biomimetic Applications," Chemistry of Materials, vol. 29, no. 10, pp. 4461–4477, May 2017, doi: 10.1021/acs.chemmater.7b01020.
48 M. R. Sala, O. Skalli, and F. Sabri, "Optimal structural and physical properties of aerogels for promoting robust neurite extension in vitro," Biomaterials Advances, vol. 135, 2022, doi: 10.1016/j.msec.2022.112682.
49 V. Serpooshan, T. M. Quinn, N. Muja, and S. N. Nazhat, "Characterization and modelling of a dense lamella formed during self-compression of fibrillar collagen gels: implications for biomimetic scaffolds," Soft Matter, vol. 7, no. 6, p. 2918, 2011, doi: 10.1039/c0sm00691b.
50 C. A. Schneider, W. S. Rasband, and K. W. Eliceiri, "NIH Image to ImageJ: 25 years of image analysis," Nat Methods, vol. 9, no. 7, pp. 671–675, Jul. 2012, doi: 10.1038/nmeth.2089.
51 Y. Yuan, "Vascularized Lung Tissue Engineering," in Reference Module in Biomedical Sciences, vol. 1, Elsevier, 2019. doi: 10.1016/B978-0-12-801238-3.65562-9.
52 B. Yi, Q. Xu, and W. Liu, "An overview of substrate stiffness guided cellular response and its applications in tissue regeneration," Bioact Mater, vol. 15, pp. 82–102, Sep. 2022, doi: 10.1016/j.bioactmat.2021.12.005.
53 O. Chaudhuri et al., "Substrate stress relaxation regulates cell spreading," Nat Commun, vol. 6, no. 1, p. 6365, Feb. 2015, doi: 10.1038/ncomms7365.
54 E. Ban et al., "Mechanisms of Plastic Deformation in Collagen Networks Induced by Cellular Forces," Biophys J, vol. 114, no. 2, pp. 450–461, Jan. 2018, doi: 10.1016/j.bpj.2017.11.3739.
55 M. P. E. Wenger, L. Bozec, M. A. Horton, and P. Mesquida, "Mechanical Properties of Collagen Fibrils," Biophys J, vol. 93, no. 4, pp. 1255–1263, Aug. 2007, doi: 10.1529/biophysj.106.103192.
56 Z. L. Shen, M. R. Dodge, H. Kahn, R. Ballarini, and S. J. Eppell, "Stress-Strain Experiments on Individual Collagen Fibrils," Biophys J, vol. 95, no. 8, pp. 3956–3963, Oct. 2008, doi: 10.1529/biophysj.107.124602.
57 M. Fang, E. L. Goldstein, E. K. Matich, B. G. Orr, and M. M. Banaszak Holl, "Type I Collagen Self-Assembly: The Roles of Substrate and Concentration," Langmuir, vol. 29, no. 7, pp. 2330–2338, Feb. 2013, doi: 10.1021/la3048104.
58 M. Raspanti, M. Viola, M. Sonaggere, M. E. Tira, and R. Tenni, "Collagen Fibril Structure Is Affected by Collagen Concentration and Decorin," Biomacromolecules, vol. 8, no. 7, pp. 2087–2091, Jul. 2007, doi: 10.1021/bm070091t.

Data is available upon request.